

Polymer electrolyte membrane resistance model

Sindhuja Renganathan, Qingzhi Guo, Vijay A. Sethuraman, John W. Weidner, Ralph E. White*

Center for Electrochemical Engineering, Department of Chemical Engineering, University of South Carolina, Columbia, SC 29208, USA

Received 2 November 2005; accepted 26 January 2006

Available online 31 March 2006

Abstract

A model and an analytical solution for the model are presented for the resistance of the polymer electrolyte membrane of a H₂/O₂ fuel cell. The solution includes the effect of the humidity of the inlet gases and the gas pressure at the anode and the cathode on the membrane resistance. The accuracy of the solution is verified by comparison with experimental data. The experiments were carried out with a Nafion 112 membrane in a homemade fuel cell test station. The membrane resistances predicted by the model agree well with those obtained during the experiments.

© 2006 Published by Elsevier B.V.

Keywords: Polymer electrolyte membrane; Membrane resistance; Fuel cell; Nafion 112; Analytical solution

1. Introduction

The pressing need for a clean, efficient and reliable power source has led to the rapid development of fuel cell technology. Fuel cells employing a polymer electrolyte membrane (PEM) are widely regarded as a potential power source for many automotive and stationary applications [1,2]. These polymer electrolyte membrane fuel cells (PEMFCs) consist of the membrane electrode assembly (MEA) and gas channels. The MEA is made up of two gas diffusion layers (GDLs), two carbon supported catalyst layers and PEM [3]. The GDLs allow the simultaneous transport of the gas (H₂ or O₂) and water from the gas channels to the catalyst layers and also serve as the current collectors. The catalyst layers (commonly Pt or the Pt alloys) provide the active sites required for the electrochemical reactions. During the MEA preparation the catalyst layer is either applied on to the GDL or on to the membrane, followed by the addition of the other component [4]. The core of the PEMFC is the membrane that is sandwiched between the catalyst layers. The PEM conducts protons from the anode to the cathode and separates the anode and the cathode gases from each other. A detailed review of some of these proton conductors and their application to fuel cells is presented by Kreuer [5]. The most commonly used membrane in the PEMFC is Du Pont's Nafion [6]. Its properties and

applications to fuel cells are extensively reported in the literature [7–10].

The conductivity of the PEM is a key factor for the performance of the fuel cell system. There are microscopic models in the literature that discuss the membrane conductivity in detail [11–18]. The conductivity, to a large extent depends on the water content of the membrane [19]. The macroscopic models available in the literature are either the diffusive flow type models [20–22] or the hydraulic flow type models [23,24]. The diffusion based models employ an empirical expression developed by Springer et al. [20] or its modified form for the water content in the membrane. The model developed by Bernardi and Verbrugge [23] forms the basis for most of the hydraulic flow type models. Apart from these models, there are also other macroscopic models that employ chemical potential as the driving force instead of specifying the flow type [25,26]. Recently a two-phase model, which includes the simultaneous presence of liquid and vapor in the membrane, was developed by Weber and Newman [27].

The present study is based on the hydraulic flow type model developed by Eikerling et al. [28], which includes a relationship between water content and the microscopic structure of the membrane. The objective of this study is to predict the ionic resistance of the membrane using a simple model and to validate it using experimental data. An attempt is made to introduce some simplifying assumptions while trying to maintain the physical insight provided by the original model.

* Corresponding author. Tel.: +1 803 777 3270; fax: +1 803 777 8265.
E-mail address: white@engr.sc.edu (R.E. White).

Nomenclature

C_W	molar concentration of water (mol m^{-3})
f	fraction of hydrophobic pores in the GDL
F	Faraday's constant (C mol^{-1})
i	current density (A cm^{-2})
I	current (A)
K^m	permeability of the PEM (m^2)
K_{abs}^d	absolute permeability of the GDL (m^2)
K_{abs}^m	absolute permeability of the PEM (m^2)
K_{rel}^d	relative permeability of the GDL
L^d	length of the GDL (m)
L^m	length of the PEM (m)
$N_{\text{H}_2}^{\text{in}}$	inlet molar flux of hydrogen ($\text{mol m}^{-2} \text{ s}$)
$N_{\text{O}_2}^{\text{in}}$	inlet molar flux of oxygen ($\text{mol m}^{-2} \text{ s}$)
$N_{\text{W}}^{\text{darcy},j}$	molar flux of water due to the Darcy's flow in the region j ($\text{mol m}^{-2} \text{ s}$)
$N_{\text{W}}^{\text{drag},j}$	molar flux of water due to the electro-osmotic drag in the region j ($\text{mol m}^{-2} \text{ s}$)
$N_{\text{W}}^{\text{in},a}$	molar flux of water at the anode GDL inlet ($\text{mol m}^{-2} \text{ s}$)
$N_{\text{W}}^{\text{in},c}$	molar flux of water at the cathode GDL inlet ($\text{mol m}^{-2} \text{ s}$)
N_{W}^m	molar flux of water in the PEM ($\text{mol m}^{-2} \text{ s}$)
$N_{\text{W}}^{\text{prod}}$	molar flux of water produced ($\text{mol m}^{-2} \text{ s}$)
p_C^j	capillary pressure in the region j (N m^{-2})
p_g^j	gas phase pressure in the region j (N m^{-2})
p_{liq}^j	liquid phase pressure in the region j (N m^{-2})
P_{W}	partial pressure of water (N m^{-2})
r_C^j	capillary radius of the region j (m)
rm^d	mean pore size of the GDL (m)
R	resistance of the membrane ($\text{m}\Omega \text{ cm}^{-2}$)
R^*	resistance of the membrane at the reference condition ($\text{m}\Omega \text{ cm}^{-2}$)
S_{W}^a	water content in the anode GDL ($\text{m}^3 \text{ m}^{-3}$)
S_{W}^c	water content in the cathode GDL ($\text{m}^3 \text{ m}^{-3}$)
T	absolute temperature (K)
$V(r)$	integral pore size distribution function for the membrane ($\text{m}^3 \text{ m}^{-3}$)
w^a	mole fraction of water leaving the anode humidifier along with hydrogen gas
w^c	mole fraction of water leaving the cathode humidifier along with oxygen gas
x	geometrical coordinates for membrane (m)
y^a	geometrical coordinates for anode GDL (m)
y^c	geometrical coordinates for cathode GDL (m)

Greek symbols

$\alpha(r)$	pore size distribution function for the GDL
γ	surface tension of water (N m^{-1})
ε	porosity of the GDL
η	potential drop across the membrane (V)
θ^j	contact angle of the region j (radian)

κ	specific conductivity of the membrane ($1 \Omega \text{ cm}^{-1}$)
κ^*	Specific conductivity of the membrane at the reference condition ($1 \Omega \text{ cm}^{-1}$)
λ	water content of the membrane ($\text{m}^3 \text{ m}^{-3}$)
λ_S	water content of the saturated membrane ($\text{m}^3 \text{ m}^{-3}$)
μ	viscosity of water ($\text{N m}^{-2} \text{ s}$)
ξ	electro osmotic drag coefficient of the membrane
σ	standard deviation of the pore size distribution in the GDL (m)
ϕ_1	effective porosity of the hydrophilic pores in the GDL
ϕ_2	effective porosity of the hydrophobic pores in the GDL

Subscripts

abs	absolute
atm	atmospheric
C	capillary
g	gas
liq	liquid
rel	relative
S	saturation
W	water

Superscripts

a	anode
c	cathode
d	GDL
drag	electro-osmotic drag
darcy	Darcy's flow
in	inlet
m	membrane

2. Experiment*2.1. Membrane electrode assembly (MEA) preparation*

Pt catalyst ink with 75 wt.% catalyst and 25 wt.% Nafion[®] (dry solids content) was prepared with commercially available 40.2 wt.% Pt on Vulcan XC-72 catalyst (E-TEK, De Nora North America Inc., NJ) and perfluorosulfonic acid-PTFE copolymer (5%, w/v, Alfa Aesar, MA). Isopropyl alcohol (99%, v/v, VWR Scientific Products) was used as the thinning solvent. The ink was mixed well for at least 8 h. ELAT electrodes (E-TEK, De Nora North America Inc., NJ) coated with carbon were used as gas diffusion layers (GDLs). The GDLs were cut into 10 cm² pieces. The catalyst ink was then sprayed onto the GDLs, air dried for 30 min and then dried at 110 °C for 10 min to evaporate any remaining solvent. The process was repeated until the targeted loading was achieved. Both the anode and the cathode sides had a loading of 0.5 mg cm⁻² of Pt. The catalyzed GDLs were then bonded to a pretreated Nafion[®] 112 membrane by hot pressing at 140 °C for 2 min at 500 psig to make the MEAs. The

MEA was assembled into the fuel cell with single channel serpentine flow field plates obtained from Fuel Cell Technologies in which 4.25 mm shims were added to the assembly to ensure a gap thickness that would provide the optimum compression of the GDL. The assembly was compressed at 200–325 psia ($1.37\text{--}2 \times 10^6 \text{ N m}^{-2}$) for 5 min. The cell was tightened with eight bolts to target a torque of 20 in.-lbs (2.25968 Nm) on each. The cell was allowed to rest for 25 min, during which time the necessary torque and compression corrections were applied so the final pressure of 200–325 psia ($1.37\text{--}2 \times 10^6 \text{ N m}^{-2}$) and bolt torque of 20 in.-lbs (2.25968 Nm) were achieved.

2.2. Measurements

High purity H_2 and ultra high purity O_2 were used as the fuel and oxidant, respectively. The flow rates were maintained at 200% of the stoichiometric requirements. The reactant gases were fully humidified ($\geq 100\%$ RH) unless otherwise specified. The cell temperature was maintained at 70°C throughout the experiments, while the anode and the cathode humidifiers were maintained at 75 and 70°C , respectively. The gas flow rates were regulated with mass flow controllers. The fuel cell was tested with a test station made at University of South Carolina. The flow diagram of the test station is shown in Fig. 1. Before collecting the performance data, the cell was operated at 0.4 V at the required stoichiometric ratios of the gases, for a minimum of 24 h. The polarization data were collected in the constant voltage mode. The data were collected with a voltage increment of 30 mV . An open circuit rest time of 2 min was allowed before collection of each data point. The contact resistances were made negligible by compressing the MEA to achieve the required pinch (0.33 mm) specified to neglect contact resistances [29]. Hence the high frequency (1 kHz) resistance

measured ($d\eta/dI = d(IR)/dI$) using a Hewlett–Packard milliohm meter (Model 4328A) is mainly attributed to the membrane resistance alone. The polarization curves and the resistance measurements were recorded using a personal computer interfaced with LABVIEW (National Instruments). The electronic load for the fuel cell system was Agilent 6060B which can handle a current up to 60 A .

3. Model description

In this section the governing equations for the PEM are simplified based on the assumptions stated below. This provides an analytical solution for the ionic resistance of the membrane. The resistance obtained using this expression is compared with experimental data. Further the analytical solution is validated by comparing the results with the numerical solution developed in a subsequent section.

3.1. Fuel cell system and basic assumptions

The fuel cell model considered here is a one-dimensional system consisting of three regions. The system contains an anode GDL and a cathode GDL in addition to the PEM.

The anode and the cathode catalyst layers are not considered explicitly and they are considered to be very thin layers of negligible thickness present at the respective GDL/PEM interfaces. The electrochemical reactions and the phase changes are considered to occur at these GDL/membrane interfaces. The schematic diagram of the system is shown in Fig. 2. The basic assumptions used in the model are given below:

- (i) The system is considered to be isothermal.
- (ii) The system is considered to be at steady state.

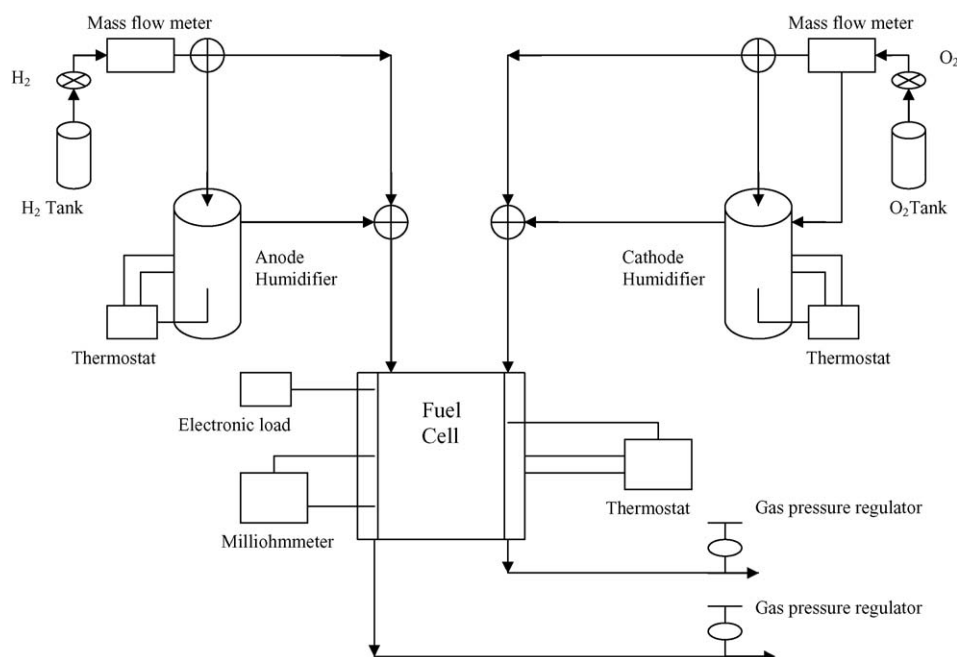


Fig. 1. Schematic representation of the fuel cell experimental setup.

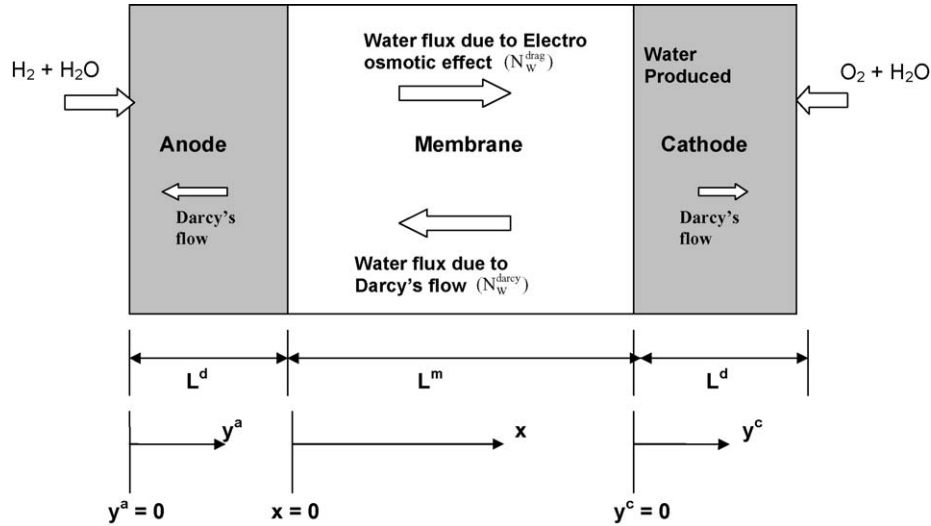


Fig. 2. Schematic representation of the fuel cell model system.

- (iii) Both the anode GDL and the cathode GDL are considered to be identical porous media.
- (iv) The PEM in this case is Nafion, a perfluorosulfonic acid membrane with a PTFE backbone [10]. The PEM is considered to have a porous structure. The sulfonic acid group separates itself from the polymer matrix and forms clusters when hydrated with water. These ionic clusters grow and form interconnecting channels, which expand to accommodate the liquid water that is in equilibrium with the membrane [13]. This gives rise to porous structure.
- (v) The pores in all the three regions of the fuel cell system are treated as cylindrical capillaries.
- (vi) The capillary framework is used for water transport in all the regions.
- (vii) The water vapor brought along with the anode and the cathode gas is assumed to condense into liquid water at the respective GDL/membrane interface. There is no phase change considered in the GDL regions.
- (viii) The water removal from the system is considered to be in the liquid phase.
- (ix) The membrane is assumed to be in equilibrium with only liquid water. No gas cross over is considered across the membrane.

There is no net water flux across the membrane (see Appendix A).

These assumptions allow us to treat liquid water transport in each region separately using capillary phenomena [28]. In the context of capillary framework, the characteristic pore size is taken as the radius of the capillary meniscus. The capillary radius (r_C) is related to the capillary pressure (p_C) and the wetting properties of the medium are given by the Laplace's expression [30]:

$$r_C^j = -\frac{2\gamma \cos(\theta^j)}{p_C}, \quad j = a, c, m \quad (1)$$

where γ is the surface tension of water and θ^j is the contact angle between water and the medium j . The capillary pressure (p_C^j) is the result of two opposing forces acting in the membrane, namely the gas phase pressure (p_g^j) and the liquid water pressure (p_{liq}^j):

$$p_C^j = p_g^j - p_{liq}^j, \quad j = a, c, m \quad (2)$$

In the following section the model of the membrane system is described in detail and an analytical solution for the membrane ionic resistance is obtained.

3.2. Membrane

3.2.1. Governing equations

The anode/membrane interface is chosen as the origin of the coordinate system for the membrane model (see Fig. 2). The transport of the protons across the membrane takes place in the presence of water. The proton drag across the membrane is described by Ohm's law [31]:

$$i = -\kappa(\lambda(p_C)) \frac{d\eta}{dx} \quad (3)$$

$$\eta = -i \int_0^{L^m} \frac{dx}{\kappa(\lambda(p_C))} \quad (4)$$

where η is the potential drop across the membrane, $\kappa(\lambda(p_C))$ the specific conductivity, which is the function of the water content, $\lambda(p_C)$ [28], which in turn is a function of the capillary pressure, p_C . A linear dependence of conductivity on water content is assumed [32]:

$$\kappa(\lambda(p_C)) = \kappa^* \lambda(p_C) \quad (5)$$

where κ^* is the specific conductivity of the membrane at the reference condition. In this study the open circuit operating condition is chosen to be the reference condition.

The flux of water in the membrane is comprised of two components. One is due to the electro-osmotic drag, i.e., the water dragged in along with the proton. This part of the water flux, N_W^{drag} is given by [27]:

$$N_W^{\text{drag}} = \frac{i\xi}{F} \quad (6)$$

Here i/F is the proton flux across the membrane and ξ is the electro-osmotic drag coefficient, which is the number of moles of water dragged along with each mole of the proton. The other part is due to the Darcy's flow [3]:

$$N_W^{\text{darcy}} = -\frac{c_W K^m(\lambda(p_C))}{\mu} \frac{dp_{\text{liq}}}{dx} \quad (7)$$

Hence the total water flux inside the membrane is given by:

$$N_W^m = \frac{i\xi}{F} - \frac{c_W K^m(\lambda(p_C))}{\mu} \frac{dp_{\text{liq}}}{dx} \quad (8)$$

The electro-osmotic drag coefficient (ξ) is assumed to be a constant [27]. For the permeability of the membrane, $K^m(\lambda(p_C))$, we adopt a linear dependence of water content, which is a reasonable approximation for thin membranes (50 μm):

$$K^m(\lambda(p_C)) = K_{\text{abs}}^m \lambda(p_C) \quad (9)$$

where K_{abs}^m is the absolute permeability of water in the membrane.

Using (2) and (8) Eq. (7) can be written as

$$N_W^m = \frac{i\xi}{F} - \frac{c_W K_{\text{abs}}^m \lambda(p_C)}{\mu} \left(\frac{d(-p_C)}{dx} + \frac{dp_g}{dx} \right) \quad (10)$$

Since we have assumed the gas crossover to be negligible, the gas pressure profile across the membrane is

$$\frac{dp_g}{dx} \approx \frac{p^a - p^c}{L^m} = \frac{\Delta p_g}{L^m} \quad (11)$$

Hence Eq. (10) yields the net water flux across the membrane, which is written as

$$N_W^m = \frac{i\xi}{F} - \frac{c_W K_{\text{abs}}^m \lambda(p_C)}{\mu} \left(\frac{d(-p_C)}{dx} + \frac{\Delta p_g}{L^m} \right) \quad (12)$$

Since the net water flux across the membrane is assumed to be zero for the all the operating conditions considered in this study (see Appendix A), Eq. (12) becomes:

$$\frac{d(-p_C)}{dx} = \frac{i\xi\mu}{c_W K_{\text{abs}}^m \lambda(p_C) F} - \frac{\Delta p_g}{L^m} \quad (13)$$

3.2.2. Membrane resistance

Eqs. (4) and (13) form the set of governing equations for the transport of species (proton and water, respectively) in the membrane. These two equations are combined to yield the following expression for potential drop across the membrane:

$$\eta = -i \int_{p_{C1}}^{p_{C2}} \frac{d(-p_C)}{(\kappa^* \lambda(p_C)) \{ ((i\xi/F)\mu) / (c_W K_{\text{abs}}^m \lambda(p_C)) - (\Delta p_g) / (L^m) \}} \quad (14)$$

where p_{C1} and p_{C2} are the capillary pressures of the anode and the cathode side of the membrane, respectively. Changing the

variable of integration from p_C to r_C and utilizing Eq. (1), Eq. (14) becomes:

$$\eta = i2\gamma \cos(\theta^m) R^* \int_{r_{C1}}^{r_{C2}} \frac{d(r_C)}{r_C^2 (\beta - \Delta p_g \lambda(r_C))} \quad (15)$$

where

$$\beta = \frac{(i\xi/F)\mu L^m}{c_W K_{\text{abs}}^m} \quad (16)$$

and

$$R^* = \frac{L^m}{\kappa^*} \quad (17)$$

Comparing Eq. (15) with Ohm's law i.e., Eq. (4), we have an expression for the membrane resistance:

$$R = -\frac{\eta}{i} = -2\gamma \cos(\theta^m) R^* \int_{r_{C1}}^{r_{C2}} \frac{d(r_C)}{r_C^2 (\beta - \Delta p_g \lambda(r_C))} \quad (18)$$

In Eq. (18) the membrane resistance R is a function of the current density (i) and water content in the membrane ($\lambda(r_C)$). In order to evaluate the membrane resistance, the water content of the membrane (λ) as a function of capillary radius (r_C) is necessary.

3.2.3. Expression for water content of the membrane

The expression for water content in the membrane is obtained by virtue of the formation of the porous structure and the definition of water content in the membrane. As mentioned before the sulfonic acid group present in the membrane side chain forms clusters and interconnecting channels in the presence of water. When liquid water enters the membrane, these channels interconnecting the clusters expand. The water content in the membrane is the fraction of the channels that has expanded to accommodate the liquid water [28]. It is determined by the integral pore size distribution function, $V(r_C)$, normalized to the saturation water content for the membrane (λ_S), which is equivalent to the maximum volume of the pores in the membrane [33]:

$$\lambda(r_C) = \frac{V(r_C)}{\lambda_S} \quad (19)$$

In the case of Nafion 112 the maximum water content is $0.44 \text{ cm}^3 \text{ cm}^{-3}$ [33].

3.2.4. Analytical solution for the membrane resistance

A straight line is fitted to the integral pore size distribution data [33] ($V(r_C)$ versus r_C) of Nafion 112. Using this relation and Eq. (19) we get the relation between the water content in the membrane and the pore radius as

$$\lambda(r_C) = 8607.3r_C + 0.6 \quad (20)$$

Using (18) and (20), we arrive at an analytical expression for the membrane resistance:

$$R = -2\gamma \cos(\theta^m) R^* \left[\ln \left(\frac{(r_{C2} - r_{C1})^{8607.3\Delta p_g/\delta^2}}{[\beta - \Delta p_g(8607.3(r_{C2} - r_{C1}) + 0.6)]^{8607.3\Delta p_g/\delta^2}} \right) - \frac{1}{\delta(r_{C2} - r_{C1})} \right] \quad (21)$$

where

$$\delta = \beta - 0.6\Delta p_g \quad (22)$$

In Eq. (21), r_{C1} and r_{C2} are the capillary radii at the membrane GDL boundaries, which are estimated using the GDL model (developed in a subsequent section).

3.2.5. Numerical solution for the membrane resistance

To estimate the accuracy of the analytical expression developed in the previous section, we have also evaluated the membrane resistance using a numerical model. In order to accomplish this task the actual integral pore size distribution data for Nafion 112 [33] is correlated with the capillary radius, r_C , and using Eq. (19) we get the membrane water content as the function of the capillary radius:

$$\lambda(r_C) = 0.978 - \frac{8.04 \times 10^{-9}}{r_C} + \frac{3.09 \times 10^{-17}}{r_C^2} - \frac{4.57 \times 10^{-26}}{r_C^3} + \frac{1.15 \times 10^{-35}}{r_C^4} + \frac{1.34 \times 10^{-44}}{r_C^5} \quad (23)$$

Eq. (23) is used along with Eq. (18) and the GDL model to obtain a numerical solution for the PEM resistance.

3.3. GDL model

The GDL is considered to be a porous medium comprising of a mixture of hydrophilic and hydrophobic pores [34]. The liquid water transport inside the GDL is considered to be only by capillary phenomena. The gas phase pressure is considered to be uniform in each GDL region. Due to the presence of gas in the medium, the flow of water is similar to that of the flow in an unsaturated medium [34].

The water flux flowing away from the membrane in the GDL is described by Darcy's flow for unsaturated medium [34], which is given as

$$N_W^{\text{dracy},j} = -\frac{c_W K_{\text{abs}}^d K_{\text{rel}}^j}{\mu} \frac{dp_{\text{liq}}^j}{dy^j}, \quad j = a, c \quad (24)$$

The relative permeability K_{rel}^j is assumed to be a cubic function of water content in the medium S_W^j , as shown by [34]. Hence we have:

$$N_W^{\text{dracy},j} = -\frac{c_W K_{\text{abs}}^d (S^j)^3}{\mu} \frac{dp_{\text{liq}}}{dy^j}, \quad j = a, c \quad (25)$$

Combining Eqs. (2) and (25) we have:

$$N_W^{\text{dracy},j} = \frac{c_W K_{\text{abs}}^d (S^j)^3}{\mu} \frac{dp_C}{dy^j}, \quad j = a, c \quad (26)$$

The water content of the GDL, S_W^j is related to the capillary pressure, p_C^j and the properties of the GDL by the following expression (see Appendices A and B):

$$S_W^j = \frac{1}{2} \left(1 + (1 - 2\phi_2) \text{erf} \left(\frac{\ln(-((2\gamma \cos \theta^d)/p_C^j)) - \ln(\text{rm}^d)}{\sigma\sqrt{2}} \right) \right), \quad j = a, c \quad (27)$$

Here ϕ_2 is the porosity of the hydrophobic pores in the GDL, γ the surface tension of water, θ^d the contact angle made by water with the GDL, rm^d the mean pore size in the GDL and σ is the standard deviation of the pore size distribution function of the GDL material.

The liquid pressure or capillary pressure profile in the anode and cathode GDL is solved using a simple water balance in the respective region. Since the water flux is assumed to be uniform in the GDL and no phase change is considered, the inlet flux of water in each region is the same as the flux of water described by Darcy's flow (away from the membrane towards the respective gas channels) for that region. In the cathode region (cathode GDL/membrane boundary) there is additional water produced due to the electrochemical reduction of oxygen. Hence we have:

$$\text{for the anode region : } N_W^{\text{dracy},a} = N_W^{\text{in},a} \quad (28)$$

$$\text{for the cathode region : } N_W^{\text{dracy},c} = N_W^{\text{in},c} + N_W^{\text{prod}} \quad (29)$$

The feed coming out of the anode and the cathode humidifiers is considered to be a binary mixture of the water vapor and H_2/O_2 gas, respectively. Fick's law of diffusion [35] is used to calculate the flux of water leaving from the humidifier along with the gases:

$$\text{for the anode : } N_W^{\text{in},a} = N_{\text{H}_2}^{\text{in}} \left(\frac{w^a}{1 - w^a} \right) \quad (30)$$

According to Faraday's law [31], $N_{\text{H}_2}^{\text{in}} = 1/2F$ is the theoretical molar flux requirement of hydrogen. Hence Eq. (30) becomes:

$$N_W^{\text{in},a} = \frac{i}{2F} \left(\frac{w^a}{1 - w^a} \right) \quad (31)$$

$$\text{and for the cathode : } N_W^{\text{in},c} = -N_{\text{O}_2}^{\text{in}} \left(\frac{w^c}{1 - w^c} \right) \quad (32)$$

where $N_{\text{O}_2}^{\text{in}} = i/4F$ is the theoretical molar flux requirement of oxygen. Hence Eq. (32) becomes:

$$N_W^{\text{in},c} = -\frac{iw^c}{4F(1 - w^c)} \quad (33)$$

Along with this the flux for water produced (according to Faraday's law [31]) in the cathode which is written as

$$N_W^{\text{prod}} = -\frac{i}{2F} \quad (34)$$

Thus water flux in cathode GDL region becomes:

$$N_W^{\text{in,c}} = -\frac{i}{2F} - \frac{iw^c}{4F(1-w^c)} \quad (35)$$

Using Eqs. (26), (28) and (31), the governing equation for the anode region becomes:

$$\frac{dp_C^a}{dy^a} = \frac{(i/2F)(w^a/(1-w^a))\mu}{c_W K_{\text{abs}}^d(S^a)} \quad (36)$$

Using Eqs. (26), (29) and (35), the governing equation for the cathode region becomes:

$$\frac{dp_C^c}{dy^c} = -\frac{((i/2F) + iw^c/(4F(1-w^c)))\mu}{c_W K_{\text{abs}}^d(S_W^c)} \quad (37)$$

At both the anode and the cathode GDL inlets (GDL/gas channel boundary), the gas and the liquid pressure continuity is assumed.

Thus we have:

$$p_g^{\text{in}} = p_g^{\text{d}} \quad (38)$$

and

$$p_{\text{liq}}^{\text{in}} = p_{\text{liq}}^{\text{d}} \quad (39)$$

Since there is no liquid in the gas channel we let the liquid pressure as zero. The capillary pressure at the GDL/gas channel boundary (GDL inlet) is given by

$$p_C^{\text{d,in}} = p_g^{\text{d,in}} - p_{\text{liq}}^{\text{d,in}} \quad (40)$$

Using (38) and (39), Eq. (40) becomes:

$$p_C^{\text{d}} = p_g^{\text{in}} - 0 \quad (41)$$

This is used as the boundary conditions to solve Eqs. (36) and (37) to obtain the pressure profiles at the anode and the cathode regions, respectively. These differential equations along with their respective boundary conditions are solved separately (dsolve, numeric) using MAPLE software. The capillary radius at a membrane/GDL boundary is calculated using the capillary pressure obtained at that boundary, and Eq. (1). These capillary radii, r_{C1} and r_{C2} obtained at the membrane boundaries are used in the calculation of the membrane resistance in Eq. (20).

4. Results and discussion

4.1. Current–voltage plots

We first discuss the effect of different operating parameters on the current–voltage performance. The current–voltage curves obtained experimentally are shown in Fig. 3. These data show an overall increase in performance upon application of gas pressure at either the anode side or the cathode side. The pressure at the anode side slightly enhances the performance. When pressure is applied to the cathode region the performance enhancement is

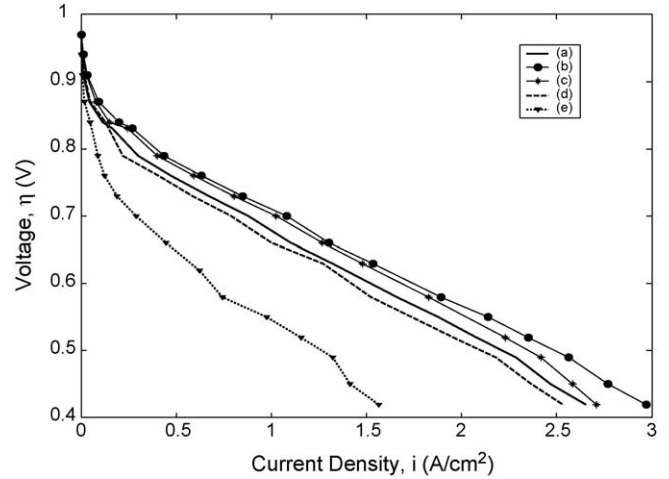


Fig. 3. Polarization curves under different operating conditions. (a) Fully humidified gases with no gas pressure at the anode and the cathode. (b) Fully humidified gases with cathode gas pressure of 2 atm. (c) Fully humidified gases with the anode gas pressure of 2 atm. (d) Dry cathode gas (O_2) with no gas pressure at the anode and the cathode. (e) Dry anode gas (H_2) with no gas pressure at the anode and the cathode.

almost to the same degree as that of the anode at lower current density region (up to 0.8 A cm^{-2}), while beyond that there is a gradual increase in the performance. When dry oxygen gas is used as the oxidant the performance decreases. There is a dramatic decrease in the performance of the fuel cell system when dry H_2 gas is used as the anode feed. The loss in voltage drop across the membrane is nearly 100 mV.

4.2. Membrane resistance

4.2.1. Resistance measured experimentally

When the fuel cell is operating under load, the data obtained from the HP milliohm meter (Model 4328A), does not give the values of the resistance directly, R , but only reflects the change in potential drop across the membrane with change in current:

$$\frac{d\eta}{dI} = \frac{d(IR)}{dI} \quad (42)$$

The potential drop across the membrane (η) for an applied current (I) is obtained by integrating Eq. (42). The area-specific membrane resistance R (expressed as product of resistance and the area of the membrane) is then obtained from this calculated potential drop at each current density, i :

$$R = -\frac{\eta}{i} = -\frac{\int_{0.01}^I (d\eta/dI)dI}{i} \quad (43)$$

4.2.2. Validation of the analytical model against the experimental data and the numerical solution

4.2.2.1. Analytical model and experimental data. The membrane resistance results (obtained using the analytical model, Eq. (21) and the experimental data) of Nafion 112 are shown in Fig. 4 as a function of the current density at 70°C . The parameters used in the model are given in Table 1. The resistance is normalized with the resistance of the membrane at open circuit condition

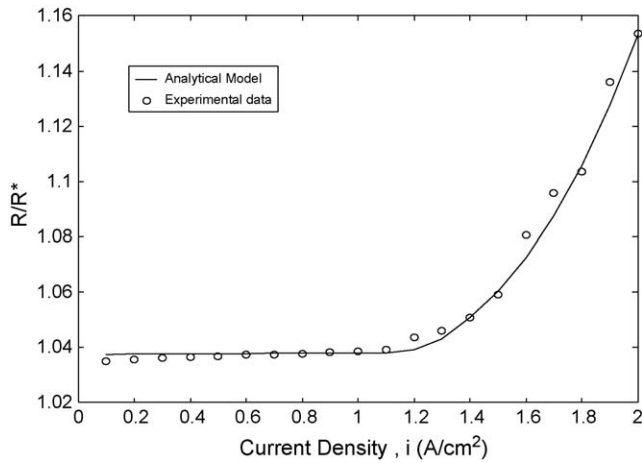


Fig. 4. Comparison of the analytical solution with the measured values for the membrane resistance of a H_2/O_2 fuel cell employing Nafion 112 membrane and operated at $70^\circ C$ with fully saturated gases and no pressure difference between the anode and the cathode.

(R^*), for facilitating comparison between the various operating conditions. In this study the resistance R^* was found to be $85 \text{ m}\Omega \text{ cm}^{-2}$. The data shown in Fig. 4 corresponds to the fully saturated feed condition with no gas pressure difference between both the anode and the cathode sides. This is chosen as the reference case for comparing the resistances obtained for all the other operating conditions considered in this study. As observed in Fig. 4, the measured (and predicted) membrane resistance is almost constant up to a current density of 1.2 A cm^{-2} . Beyond

this point there is a sharp increase in the resistance of the membrane, with an increase in the current density. This increase in the resistance is approximately 10% ($\sim 8.5 \text{ m}\Omega \text{ cm}^{-2}$), when the current density increases from 1.2 to 2.0 A cm^{-2} . A constant value of the resistance with has been reported in literature [36] for thin membranes ($60 \mu\text{m}$). For Nafion 117 ($\sim 200 \mu\text{m}$), a noticeable increase in the membrane resistance with an increase in the current density has been reported [37] even at much lower current density region (0.2 – 0.7 A cm^{-2}) and this is attributed to the partial dehydration of the membrane. The sharp increase in the resistance value found in this study at higher current densities indicates the possibility of partial membrane dehydration at these current densities even for thin membranes ($50 \mu\text{m}$). The analytical model developed here is able to predict this trend in the membrane resistance to a remarkable extent (within 1% error).

The term β in Eq. (15) which is a measure of the electro-osmotic drag, increases with the increase in the current density. The difference in the capillary radius ($r_{C2} - r_{C1}$) is the measure of the water brought into the membrane by the Darcy's flow. The greater the difference in the capillary radius the less water is brought into the membrane. The GDL model (Eqs. (36) and (37)) predicts an increase in the difference of the capillary pressure with an increase in the current density. This in turn results in a decrease in the difference of the radius at the two membrane boundaries. Before the critical current density (1.2 A cm^{-2} in this study) is reached, the water loss at the anode side of the membrane due to the electro-osmotic drag is compensated by the water brought in by Darcy's flow resulting in uniform water content across the membrane and a constant resistance. With the

Table 1
Parameter values used in this study

Parameter	Symbol	Value/expression	S.I. unit	Reference
Cell Temperature	T	353	K	*
Porosity of the GDL	ε	0.4	–	[40]
Length of the GDL	L^d	2.5×10^{-4}	m	[41]
Length of the membrane	L^m	50×10^{-6}	m	**
Absolute permeability of the GDL	K_{abs}^d	7×10^{-6}	m^2	[40]
Mean radius of the GDL	r_{m}^d	1.37×10^{-6}	m	[40]
Contact angle of water with the GDL	θ^d	2.61	radian	[41]
Fraction of the hydrophobic pores in the GDL	f^d	0.98	–	[40]
Standard deviation of the pore size distribution in the GDL	σ^d	2.44×10^{-6}	m	[40]
Contact angle of water with the membrane	θ^m	1.5711	radian	[27]
Partial pressure of water	p_w	$\exp\left(11.6832 - \frac{3816.44}{T - 46.13}\right) \times 10^5$	N m^{-2}	[42]
Molar concentration of water	C_w	$\frac{18}{1.1.603 - 0.0005371T}$	mol m^{-3}	[42]
Viscosity of water	μ	$(2695.3 - 6.6T) \times 10^{-6}$	Pa s^{-1}	[42]
Surface Tension of water	γ	$(0.12398 - 0.000173937T)$	N m^{-1}	[41]
Electro osmotic drag coefficient of the membrane	ξ	$2.55 \exp\left(\frac{4000}{8.314} \left(\frac{1}{303.15} - \frac{1}{T}\right)\right)$	–	[27]
Faraday's constant	F	96487	C	[31]
Absolute permeability of the membrane	K_{abs}^m	5.2×10^{-20}	m^2	[43]
Maximum water content in the membrane	λ_s	0.44	$\text{m}^3 \text{ m}^{-3}$	[33]
Resistance of the membrane at reference condition	R^a	8.5	$\text{m}\Omega \text{ cm}^{-2}$	**
Atmospheric pressure	p_{atm}	1.023×10^5	N m^{-2}	*
Temperature of anode humidifier	T^a	358	K	*
Temperature of cathode humidifier	T^c	353	K	*

* Operating conditions.

** Measured value.

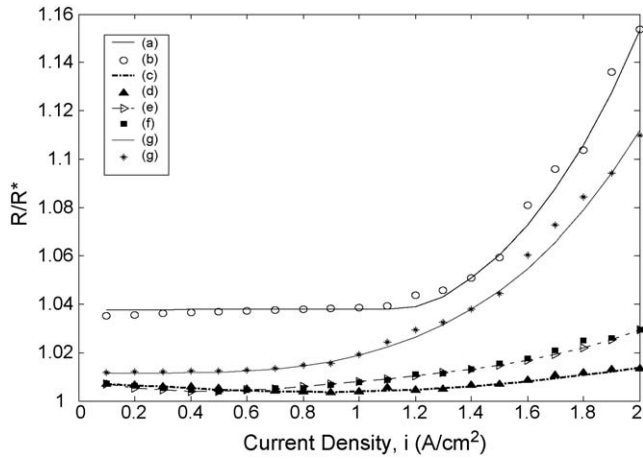


Fig. 5. Comparison of the analytical solution with the measured values for the membrane resistance of a H_2/O_2 fuel cell employing Nafion 112 membrane and operated at 70°C with fully saturated gases. (a) No cathode gas pressure (analytical model), (b) no cathode gas pressure (experimental data), (c) cathode gas pressure of 0.5 atm (analytical model), (d) cathode gas pressure of 0.5 atm (experimental data), (e) cathode gas pressure of 1.0 atm (analytical model), (f) cathode gas pressure of 1 atm (experimental data), (g) cathode gas pressure of 2 atm (analytical model), and (h) cathode gas pressure of 2 atm (experimental data).

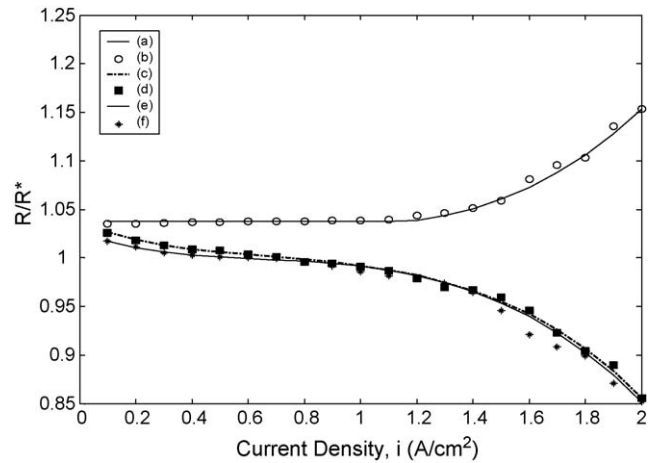


Fig. 6. Comparison of the analytical solution with the measured values for the membrane resistance of a H_2/O_2 fuel cell employing Nafion 112 membrane and operated at 70°C with fully saturated gases. (a) No anode gas pressure (analytical model), (b) no anode gas pressure (experimental data), (c) anode gas pressure of 0.5 atm (analytical model), (d) anode gas pressure of 0.5 atm (experimental data), (e) anode gas pressure of 2.0 atm (analytical model), and (f) anode gas pressure of 2 atm (experimental data).

increase in the current density the electro-osmotic drag becomes predominant thereby causing less water content in the membrane and higher resistance. The critical current density (the point of onset of the membrane partial dehydration), depends on the membrane properties and the operating conditions.

The resistance of the membrane as a function of current density for different cathode gas pressures is shown in Fig. 5. These results show that there is an increase in resistance with the increase in the current density at all cathode gas pressure values. When the pressure is 2 atm (highest pressure considered in this study), there is a pronounced increase (10%) in the resistance with an increase in the current density. But at the lower cathode pressure conditions (0.5 and 1 atm) the increase in resistance is not much pronounced. Another interesting observation is that in all these three cases the resistance values are less than the resistance obtained at the reference case considered (no cathode pressure). All these observations can be explained using the model developed. The electro-osmotic drag increases with increase in the current density, causing a water content gradient across the membrane. Darcy's flow reduces this water content gradient. As in the case of no pressure difference across the membrane, the increase in current density increases the capillary pressure gradient across the membrane. This increase in the capillary pressure gradient helps acts as a driving force for the Darcy's flow. But at higher current densities (close to 2 A cm^{-2}) the electro-osmotic drag exceeds the Darcy's flow. The application of a small pressure at the cathode acts as an additional driving force and pumps more water into the membrane at higher current densities, thus effectively decreasing the membrane resistance. When relatively higher pressure (2 atm) is applied the capillary pressure difference and hence the water content gradient across the membrane becomes significantly larger at higher current densities and this is not compensated

by the additional convective driving force provided by the difference in gas pressure.

The effect of anode gas pressure on the membrane resistance at 70°C is depicted in Fig. 6. We observe a decrease in the membrane resistance (approximately 17%) with an increase in the current density from 0.1 to 2 A cm^{-2} . This decrease in the membrane resistance with increase in the current density is nearly the same for both low and high anode gas pressures considered in this study. When we analyze the situation using the model, we find that with the application of pressure at the anode the capillary pressure at the anode side of the membrane increases resulting in increase in water content on the anode side. This complements the Darcy's flow in compensating the water loss due to the electro-osmotic drag, ensuring low membrane resistance.

Fig. 7 shows the resistance of the membrane as a function of current density when dry O_2 gas is used as the oxidant. In this case, the resistance decreases gradually from about 36% more than the corresponding reference case value to almost equal value to that of the reference case when the current density is increased from 0.1 to 2 A cm^{-2} . In the lower current density region the water flux by Darcy's flow is comparatively less due to less water content gradient across the membrane. Thus the water dragged into the PEM by the proton, which only depends on the operating current density is higher than the flow of water from the cathode to the anode, giving rise to a higher value of resistance than the reference case. This loss is gradually compensated by the increased production of water at the cathode which increases the water content gradient across the membrane aiding in more flux of water into the membrane due to the Darcy's flow.

Fig. 8 shows the membrane resistance for the case of dry H_2 gas and fully saturated cathode gas with no pressure difference between the anode and the cathode. At all current densities the resistance is larger than the reference case. This can be

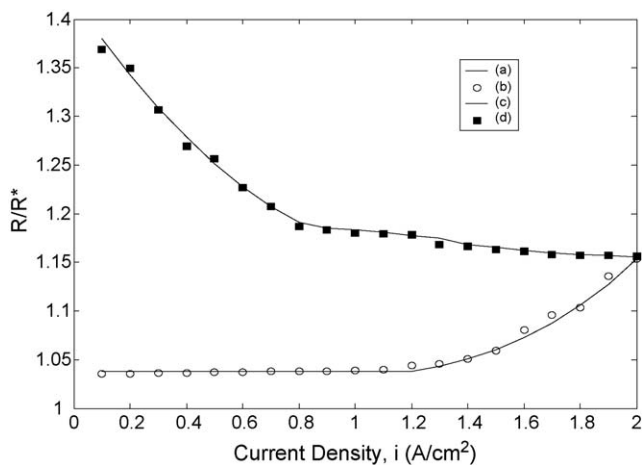


Fig. 7. Comparison of the analytical solution with the measured values for the membrane resistance of a H_2/O_2 fuel cell employing Nafion 112 membrane and operated at $70^\circ C$ with no pressure difference between the anode and the cathode. (a) Fully humidified gases (analytical model), (b) fully humidified gases (experimental data), (c) dry cathode gas (O_2) (analytical model), and (d) dry cathode gas (O_2) (experimental data).

explained by the unequal compensation of water loss due to electro-osmosis by the Darcy's flow. Water is brought into the membrane from the cathode by Darcy's flow and the proton drags water from the anode side along with it toward the cathode (electro-osmotic drag). Since there is no water present at the anode membrane boundary, the water brought in by the Darcy's flow is dragged back towards the cathode, resulting in severe dehydration of the anode side of the membrane and hence high membrane resistance. This effect is significantly reduced with an increase in the current density as more and more water is produced at the cathode and relatively more water is dragged by Darcy's flow from the cathode side to the anode. This can be observed from Eq. (21). With increase in current density the capillary radius decreases sharply and thereby increasing the dif-

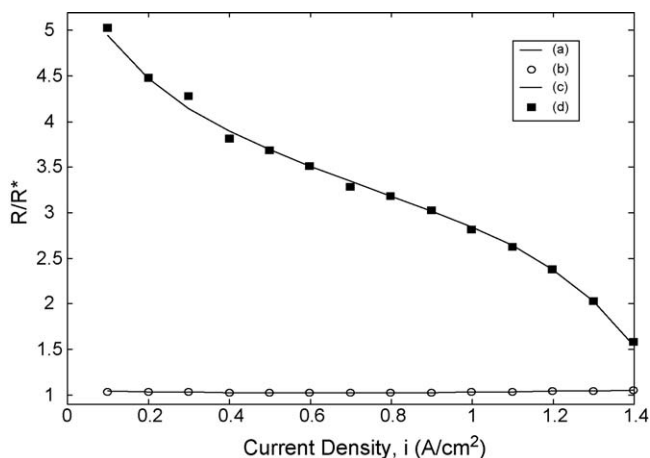


Fig. 8. Comparison of the analytical solution with the measured values for the membrane resistance of a H_2/O_2 fuel cell employing Nafion 112 membrane and operated at $70^\circ C$ with no pressure difference between the anode and the cathode. (a) Fully humidified gases (analytical model), (b) fully humidified gases (experimental data), (c) dry anode gas (H_2) (analytical model), and (d) dry anode gas (H_2) (experimental data).

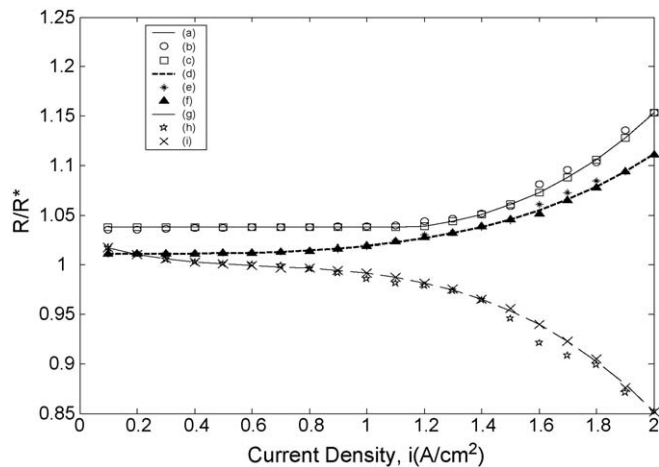


Fig. 9. Comparison of numerical solutions with the measured values and the analytical solution for the membrane resistance of a H_2/O_2 fuel cell employing Nafion 112 membrane and operated at $70^\circ C$ with fully humidified gases. (a) No gas pressure at the anode and the cathode (analytical model), (b) no gas pressure at the anode and the cathode (experimental data), (c) no gas pressure at the anode and the cathode (numerical model), (d) cathode gas pressure of 2 atm (analytical model), (e) cathode gas pressure of 2 atm (experimental data), (f) cathode gas pressure of 2 atm (numerical model), (g) anode gas pressure of 2 atm (analytical model), (h) anode gas pressure of 2 atm (experimental data), and (i) anode gas pressure of 2 atm (numerical model).

ference in the capillary radius between anode and cathode side, causing the resistance to drop.

Hence the optimum condition for fuel cell from the point of view of membrane performance, is operating the system with no or minimum humidity of the cathode gas, with the application of a small pressure at the cathode (around 0.5 atm) and comparatively large pressure (around 2 atm) at the anode with fully humidified anode gas.

4.2.2.2. Comparison of analytical, numerical solution with experimental data. Fig. 9 presents a comparison of the numerical solution (Eq. (18) along with Eq. (23)) with the analytical solution (21) and the experimental data for three different operating conditions. It is shown that when there is no pressure difference between the anode and the cathode the numerical solution and the analytical approximation are identical. But when the pressure difference exists, the numerical solution is relatively close (error is less than 1%) to the experimental data, while the analytical solution differs by 3% from the experimental data. But this small difference should not prevent us from taking advantage of the analytical solution. The approximate analytical solution can reduce the computational time in a full-scale model.

5. Conclusion

The resistance of Nafion 112 membrane was investigated under different operating conditions. It was observed that though application of pressure at both the anode side and the cathode side helps in increasing the performance of the cell, pressure at the anode helps to reduce the membrane resistance to a larger extent. The effect of dry and fully humidified gases on the membrane performance was studied. It was observed that anode

humidity decreases the membrane performance. The optimum operating pressure conditions were predicted using the analytical expression developed for the membrane resistance. Also a simple model to predict the membrane resistance was developed which was able to predict the trend in the PEM resistance with good accuracy and also provides certain physical insight for better membrane performance.

Acknowledgement

The authors are grateful for the financial support for this project by the US Department of Energy, grant/contract no. DE-FC36-04GO14232.

Appendix A

A.1. Calculation of water flux across the membrane

The flux of water in the anode (same as the flux of water at the inlet of anode GDL) is given by

$$N_{\text{W}}^{\text{in,a}} = \frac{i}{2F} \left(\frac{w^{\text{a}}}{1 - w^{\text{a}}} \right) \quad (\text{A.1})$$

where w^{a} is the moles of water leaving the anode humidifier. w^{a} at the operating temperature of the anode humidifier (75 °C) is numerically equal to 0.3743. Hence at the flux of water in the GDL is

$$N_{\text{W}}^{\text{in,a}} = \frac{0.3i}{F} \quad (\text{A.2})$$

The flux of water due to electro-osmotic drag across the membrane is given by

$$N_{\text{W}}^{\text{drag}} = \frac{i\xi}{F} \quad (\text{A.3})$$

For the Nafion membrane equilibrated with liquid water the electro-osmotic coefficient is given as 2.55 [27]. Hence the flux of water due to electro-osmotic drag is

$$N_{\text{W}}^{\text{drag}} \approx \frac{2.55i}{F} \quad (\text{A.4})$$

At all operating current densities, the flux due to the electro-osmotic drag (A.4) is greater than the flux of water at the anode side of the membrane (A.2). This ensures that the water brought into the membrane from the cathode does not flow into the anode, but only humidifies the anode side of the membrane. Thus the net water flux across the membrane is negligible at the current operating conditions.

Appendix B

The GDL is considered to be a porous medium with both hydrophilic and hydrophobic pores. The relationship between the capillary radius and water content is derived based on the concept of wetting [38]. The critical radius required for water to wet the pores depends on the nature of the pore. In the case of hydrophilic pores, the radii below the critical radius are filled

with water while in hydrophobic pores the pores above the critical radius are filled with water. This concept lets us fix the limits of integration in both the case. The approach followed here is similar to that of White et al. [39]. Here the pore size distribution function is assumed to be uniform for both the type of pores.

B.1. Derivation of water content of the GDL

Pore size distribution for hydrophilic gas pores is given by

$$\psi_1(r) = \int_{r_c}^{\infty} \alpha(r) dr \quad (\text{B.1})$$

where the pore size distribution function is assumed to be (based on the fit obtained from typical pore size distribution data for the GDL material [40]):

$$\alpha(r) = \frac{1}{r\sigma\sqrt{2\pi}} \exp \left(- \left(\frac{\ln r - \ln r_m^{\text{d}}}{\sqrt{2}\sigma} \right)^2 \right) \quad (\text{B.2})$$

Hence upon integration:

$$\psi_1(r'_c) = \frac{1 - \text{erf}(r'_c)}{2} \quad (\text{B.3})$$

where r'_c is $((\ln r_c - \ln r_m^{\text{d}})/\sqrt{2}\sigma)$

Pore size distribution for hydrophobic gas pores is given by

$$\psi_2(r) = \int_0^{r_c} \alpha(r) dr \quad (\text{B.4})$$

where the pore size distribution function is assumed to be the same log normal distribution.

Now we get:

$$\psi_2(r'_c) = \frac{1 + \text{erf}(r'_c)}{2} \quad (\text{B.5})$$

The fraction of the hydrophilic pores filled with gas or the effective hydrophilic porosity is

$$\phi_1 = \varepsilon(1 - f)\psi_1(r'_c) \quad (\text{B.6})$$

where ε is the porosity of the GDL and f is the fraction of hydrophobic pores in the GDL media. And for hydrophobic pores:

$$\phi_2 = \varepsilon f \psi_2(r'_c) \quad (\text{B.7})$$

Total fraction of pores filled with gas is

$$\phi_{\text{T}} = \phi_1 + \phi_2 = 1 \quad (\text{B.8})$$

Hence the total gas filled pores, is given by

$$\phi_{\text{T}} = \frac{1 - \text{erf}(r'_c)(1 - 2\phi_2)}{2} \quad (\text{B.9})$$

The liquid water saturation or the water content of the medium is the fraction of pores filled with water which is $1 - \phi_{\text{T}}$ and

substituting for r_C we have:

$$S_w = \frac{1}{2} \left(1 + (1 - 2\phi_2) \operatorname{erf} \left(\frac{\ln(-(2\gamma \cos \theta)/p_C) - \ln(rm^d)}{\sigma\sqrt{2}} \right) \right) \quad (\text{B.10})$$

This expression is used in the GDL model for relating the GDL properties and the water content in the medium.

References

- [1] P. Costamagna, S. Srinivasan, *J. Power Sources* 102 (2001) 242.
- [2] M.L. Perry, T.F. Fuller, *J. Electrochem. Soc.* 149 (2002) S59.
- [3] J.H. Hirschenhofer, D.B. Stauffer, R.R. Engleman, M.G. Klett, *Fuel cell Handbook*, 4th ed., Parsons Corporation, PA, 1998.
- [4] V. Mehta, J.S. Cooper, *J. Power Sources* 114 (2003) 32.
- [5] K.D. Kreuer, *Chem. Mater.* 8 (1996) 610.
- [6] O. Savadogo, *J. New Mater. Electrochem. Syst.* 1 (1998) 47.
- [7] T.D. Gierke, G.E. Munn, F.C. Wilson, *J. Polym. Sci.* 19 (1981) 1687.
- [8] T.A. Zawodinski, M. Neemann, L.O. Sillerud, S. Gottesfeld, *J. Phys. Chem.* 95 (1991) 1040.
- [9] K.A. Mauritz, R.B. Moore, *Chem. Rev.* 104 (2004) 4535.
- [10] K.D. Kreuer, S.J. Paddison, E. Spohr, M. Schuster, *Chem. Rev.* 104 (2004) 4637.
- [11] S.J. Paddison, R. Paul, T.A. Zawodinski, *J. Electrochem. Soc.* 147 (2000) 617.
- [12] P. Cormmer, A.G. Cherstvy, E. Spohr, A.A. Kornyshev, *Fuel cells* 2 (2002) 127.
- [13] W.Y. Hsu, T.D. Gierke, *J. Membr. Sci.* 13 (1983) 307.
- [14] H.L. Yeager, A. Steck, *J. Electrochem. Soc.* 128 (1981) 1880.
- [15] M. Eikerling, A.A. Kornyshev, U. Stimming, *J. Phys. Chem. B* 101 (1997) 10807.
- [16] Y. Yang, P.N. Pintauro, *AIChE. J.* 46 (2000) 1177.
- [17] P. Choi, N.H. Jalani, R. Datta, *J. Electrochem. Soc.* 152 (2005) E123.
- [18] J. Fimrite, B. Carnes, H. Struchtrup, N. Djilali, *J. Electrochem. Soc.* 152 (2005) A1815.
- [19] A.V. Anantaraman, C.L. Gardner, *J. Electroanal. Chem.* 414 (1996) 115.
- [20] T.E. Springer, T.A. Zawodinski, S. Gottesfeld, *J. Electrochem. Soc.* 138 (1991) 2334.
- [21] J.T. Wang, R.F. Savinell, *Electrochim. Acta* 37 (1992) 2737.
- [22] T.V. Nguyen, R.E. White, *J. Electrochem. Soc.* 140 (1993) 2178.
- [23] D.M. Bernardi, M.W. Verbrugge, *J. Electrochem. Soc.* 139 (1992) 2477.
- [24] G. Murgia, L. Pisani, M. Valentini, B. D'Aguanno, *J. Electrochem. Soc.* 149 (2002) A31.
- [25] T. Thampan, S. Malhortra, H. Tang, R. Datta, *J. Electrochem. Soc.* 147 (2000) 3242.
- [26] G.J.M. Janssen, *J. Electrochem. Soc.* 148 (2001) A1313.
- [27] A.Z. Weber, J. Newman, *J. Electrochem. Soc.* 151 (2004) A311.
- [28] M. Eikerling, Y.I. Kharkats, A.A. Kornyshev, Y.M. Volfkovich, *J. Electrochem. Soc.* 145 (1998) 2684.
- [29] M.V. Williams, H.R. Kunz, J.M. Fenton, *J. Electrochem. Soc.* 152 (2005) A635.
- [30] F.A.L. Dullien, in: K. Vafai, H.A. Hadim (Eds.), *Handbook of Porous Media*, Marcel Dekker Inc., New York, 2000, p. 54.
- [31] J.S. Newman, K.E. Thomas-Alyea, *Electrochemical Systems*, 3rd ed., John Wiley & sons Inc., New York, 2004.
- [32] R.F. Silva, M.D. Francesco, A. Pozio, *J. Power Sources* 134 (2004) 18.
- [33] J. Divisek, M. Eikerling, V. Mazin, H. Schmitz, U. Stimming, Y.M. Volfkovich, *J. Electrochem. Soc.* 145 (1998) 2677.
- [34] U. Pasaogullari, C.Y. Wang, *Electrochim. Acta* 49 (2004) 4359.
- [35] R.B. Bird, W.E. Stewart, E.N. Lightfoot, *Transport Phenomena*, 2nd ed., John Wiley & sons Inc., New York, 2002.
- [36] M. Watanabe, H. Uchida, M. Emori, *J. Electrochem. Soc.* 145 (1998) 1137.
- [37] F.N. Buchi, G.G. Scherer, *J. Electroanal. Chem.* 404 (1996) 37.
- [38] J.C. Berg, *Wettability*, Marcel Dekker Inc., New York, 1993.
- [39] R.E. White, M.A. Nicholson, L.G. Kleine, J. Van Zee, R. Darby, *J. Electrochem. Soc.* 131 (1984) 268.
- [40] M.V. Williams, E. Begg, L. Bonville, H.R. Kunz, J.M. Fenton, *J. Electrochem. Soc.* 151 (2004) A1173.
- [41] J. Itonen, M. Mikkola, G. Lindbergh, *J. Electrochem. Soc.* 151 (2004) A115.
- [42] F.P. Incropera, D.P. Dewitt, *Fundamentals of Heat and Mass Transfer*, 3rd ed., John Wiley & sons, New York, 1990.
- [43] F. Meier, G. Eigenberger, *Electrochim. Acta* 49 (2004) 1731.